Heliyon 9 (2023) e16740

Contents lists available at ScienceDirect

Heliyon

journal homepage: www.cell.com/heliyon

Investigating the potential of organic semiconductor materials by DFT and TD-DFT calculations on aNDTs

B. Jothi [a], A. David Stephen [b], K. Selvaraju [a,*], Abdullah G. Al-Sehemi [c]

[a] Department of Physics, Kandaswami Kandar's College, Velur, Tamilnadu, India
[b] Department of Physics, PSG College of Arts & Science, Coimbatore, Tamilnadu, India
[c] Department of Chemistry, King Khalid University, Abha, 61413, Saudi Arabia

ARTICLE INFO

Keywords:
aNDT
Absorption spectra
Crystal structure prediction
Organic semiconductor

ABSTRACT

The effects of substituting electron withdrawing and electron donating functional groups on the electronic and optical properties of angular naphthodithiophene (aNDT) were studied. Substitutions were made to the aNDT molecule at position 2 and 7, respectively. The computed ionization parameters and reorganisation energies distinguished between the p-type and n-type semiconducting natures of the unsubstituted aNDT molecule and those with the $–C_2H_5$, $–OCH_3$, $–NO_2$, and –CN substituents. However, the aNDT molecule with C_2H_5 as a substitution showed p-type behaviour since it had the largest electron reorganisation energy of about 0.37 eV. The ambipolar semiconducting property of methoxy [$–OCH_3–$] substituted aNDT molecule was revealed from the RMSD value of 0.03 Å for both positive and negative charges with respect to neutral geometry. The absorption spectra differ significantly from those of unsubstituted aNDT, which reveals the impact of functional group substitution that changes the energy level of the molecules. The maximum absorption (λ_{max}) and oscillator strength (f) at the excited states in vacuum was investigated using time dependent density functional theory (TD-DFT). The aNDT with electron withdrawing group [$-NO_2$] substitution has a maximum absorption wavelength of 408 nm. Studying the intermolecular interactions between aNDT molecules was also accomplished with the help of Hirshfeld surface analysis. The current work provides insight into the development of novel organic semiconductors.

1. Introduction

Donor-acceptor (D-A) copolymers have been widely used in organic photovoltaic (OPV) [1] and organic field-effect transistor (OFET) [2] devices because of their good solution processability and simple molecular property tuning [3–7]. This has led to the development of numerous unique, electron-rich conjugated building blocks for polymerization. Tetracyclic naphthodithiophenes (NDTs), in contrast to the tricyclic benzodithiophene derivatives, which constitute the most effective component for creating high-performance D-A copolymers of OPVs, ref. [8], are also gaining popularity due to their prolonged conjugation and variety of structures. The NDT derivatives can have isomeric structures that are either linear (lNDT) or angular (aNDT) depending on the molecular geometry [9] (Fig. 1). aNDT-based copolymers were discovered to have higher ordered structures than lNDT-based copolymers, leading to higher OFET mobilities [10]. Additionally, compared to their lNDT counterparts, the aNDT molecules have lower lying

* Corresponding author.
E-mail address: selvarajudocs@gmail.com (K. Selvaraju).

https://doi.org/10.1016/j.heliyon.2023.e16740
Received 20 February 2023; Received in revised form 24 May 2023; Accepted 25 May 2023
Available online 26 May 2023

HOMO energy levels [11], which is advantageous for improved air stability and higher open-circuit voltage (Voc) for applications in optoelectronics. Side-chain engineering, which involves adding various substituents to an aNDT framework, is crucial to maximising the use of aNDT-containing polymers for optoelectronic applications since it not only ensures solution processability but also induces the right molecular packing. One proven method for improving the optical and charge transport properties of organic molecules is to replace hydrogen atoms with either electron-withdrawing (EWG) or electron-donating (EDG) [12–14]. Takimiya and Osaka originally added two alkyl groups to the outside locations (5,10) of the core naphthalene moiety in the aNDT to address the problem [15,16]. The 5,10-dialkyl aNDT-based copolymer demonstrated superior solubility and orientational order in comparison to the polymer containing unsubstituted aNDT units, yielding a remarkable power conversion efficiency (PCE) of over 8% [17]. A 4,9-dialkoxy aNDT-based D-A copolymer with average solar cell capabilities was described by Shi et al. [18,19]. To further explore the impact of substituents on the electrical and structural characteristics of the resultant copolymers, it is desirable to further formulate another isomeric structure, 2, 7-dialkyl-aNDT. With respect to this, we have created a practical approach to regiospecifically implant electron donating and electron with drawing groups at 2,7-positions of an aNDT unit, which could have good yield in the reported synthesisation [9]. In this context, we have substituted electron donating groups; ethane (-C_2H_5) and methoxy(-OCH_3) as aNDT1 and aNDT2 respectively. Also, the electron with drawing groups; nitrite (-NO_2) and a cyano (-CN) groups were substituted at 2,7 positions in aNDT as aNDT-3 and aNDT-4 respectively. Systematically examined were the electronic and optical characteristics of unsubstituted and substituted aNDTs. First, the reorganisation energy related to charge transport was assessed using the adiabatic potential energy surface (APS) method. This method provides a good assessment of the effects of various groups on the reorganisation energy. The steady-state absorption spectra were ultimately computed with a view toward their use in optoelectronics.

2. Computational and theoretical methods

The benchmarking calculations were performed with different density functional theory [DFT] based on the available experimental result [9,14,20–22] for the isomers of aNDT molecule. It was found that the absorption maximum (λ_{max}) obtained with the Becke, 3-parameter, Lee-Yang-Parr (B3LYP) [23–25] functional and the 6−311+G (d, p) basis set is comparable with the experimental value [Table S1]. Therefore, through the use of the B3LYP/6−311+G(d,p), the structures of aNDTs were optimized and the reorganisation energy and ionization parameters were calculated. The same-level theoretical frequency calculations show that all molecules under study have hit local minima with no negative frequencies. Calculations were done for the energy gap (E_g), HOMO and LUMO energy levels. The following equation (1) [26] is used to compute the reorganisation energy for holes (λ_+) and electrons (λ_-):

$$\lambda_{\pm} = (E^{\pm}(g^{o}) - E^{\pm}(g^{\pm})) + (E^{o}(g^{\pm}) - E^{o}(g^{o})) \quad (1)$$

here, $E^{\pm}(g^0)$ is the total energy of an ion in optimized neutral geometry, $E^{\pm}(g^{\pm})$ is the energy of an ion in optimized ionic geometry, $E^0(g^{\pm})$ is the energy of the neutral molecule in ionic geometry, and $E^0(g^0)$ is the optimized ground state energy of the neutral molecule.

The following equations (2)–(7) [27] were used to determine the ionization potential (IP), electron affinity (EA), hole extraction potential (HEP), and electron extraction potential (EEP) of the aNDT-based compounds under study.

$$VIP = E^{+}(g^{0}) - E^{0}(g^{0}) \quad (2)$$

$$AIP = E^{+}(g^{+}) - E^{0}(g^{0}) \quad (3)$$

$$VEA = E^{0}(g^{0}) - E^{-}(g^{0}) \quad (4)$$

$$AEA = E^{0}(g^{0}) - E^{-}(g^{-}) \quad (5)$$

$$HEP = E^{+}(g^{+}) - E^{0}(g^{+}) \quad (6)$$

$$EEP = E^{0}(g^{-}) - E^{-}(g^{-}) \quad (7)$$

Time-dependent density functional theory (TD-DFT) with the B3LYP functional and 6–311+(d, p) basis set from ground state

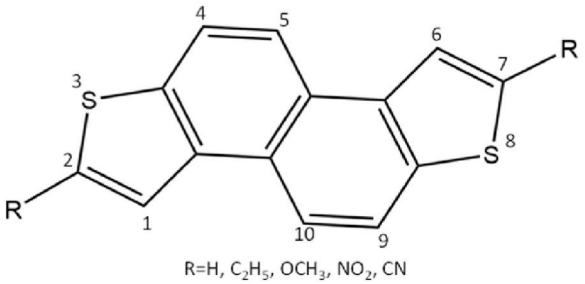

Fig. 1. The Chemical structures of aNDT's.

optimized geometry was used to determine the molecules' excited states in gas phase. This provides the molar absorption coefficient, oscillator strength and absorption spectra. The Gaussian09 [28] programme was used for all calculations. Additionally, using a Hirshfeld surface analysis [29], the intermolecular interactions between the molecules in the crystal structure were examined to assess their contribution to the crystal lattice. The $d_{i/e}$ map, shape index, and 2D fingerprint plots were displayed to aid in the analysis of the interactions. The CrystalExplorer17 programme [30] was used to perform these calculations.

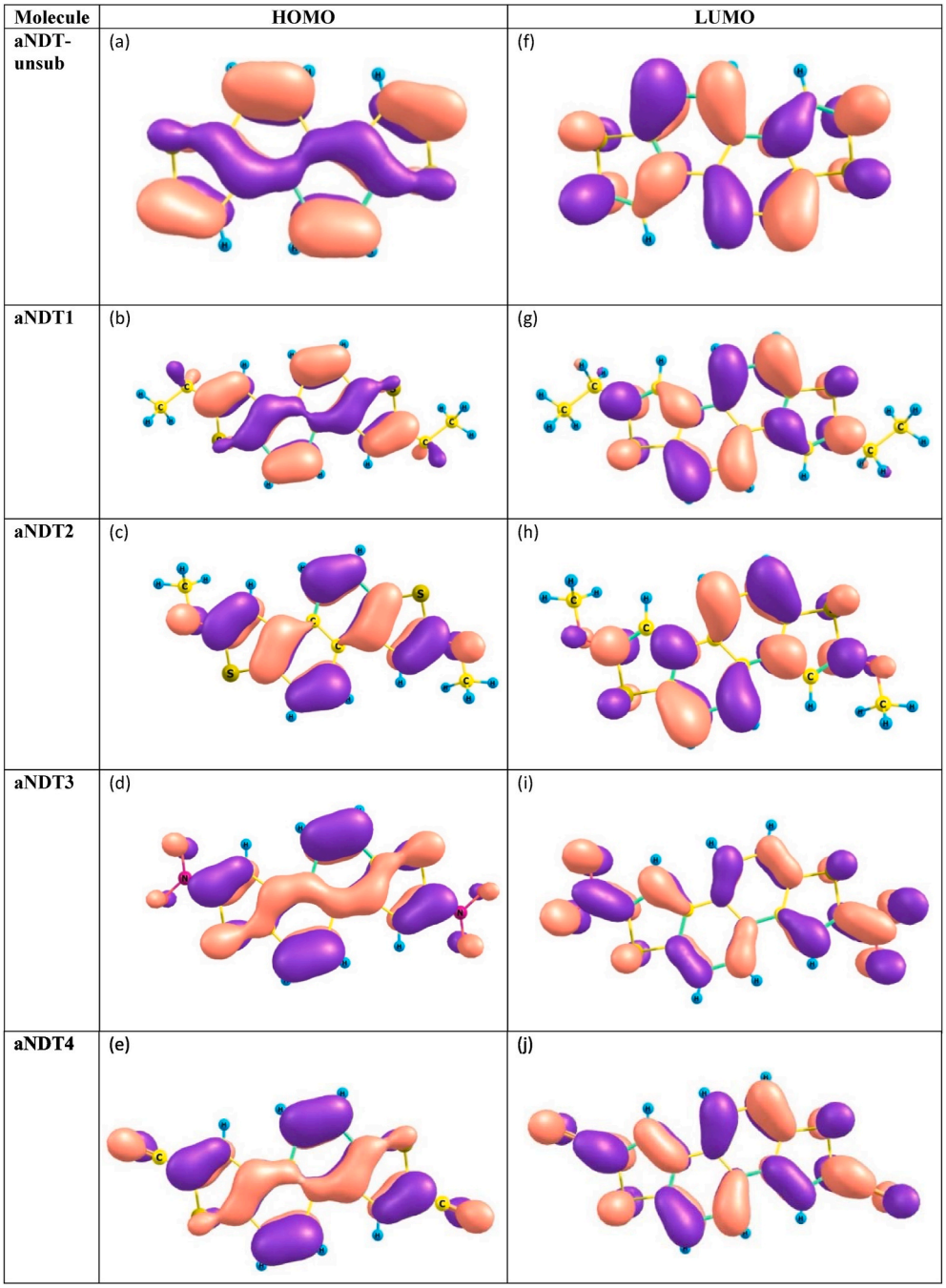

Fig. 2. HOMO (a–e) and LUMO (f–j) of unsubstituted and functionalized aNDTs.

3. Results and discussion

3.1. Frontier molecular orbitals and absorption spectra

The delocalization of electron density on the frontier molecular orbitals of the individual molecules has a significant impact on the charge transport and optical absorption characteristics of the π-stacked organic molecules. Fig. 2 displays the density map of the examined aNDT-based molecules' HOMO and LUMO calculated at the B3LYP/6−311+G(d,p) level of theory. It is noted that the HOMO of aNDT1 and aNDT2 having electron donating functionalized groups are localized on naphthalene and cyclopentane rings, while that of aNDT3 and aNDT4 with electron with drawing substitution, it is shifted to functionalized regions. The similar trend was observed in the LUMO of aNDT's and its functional derivatives. This indicates that the aNDT molecule created the charge transfer states.

Fig. 3 displays the energy band gap (E_g), HOMO, and LUMO values for aNDT, and their functionalized compounds. The E_g values of all the aNDT derivatives were fall into the 1.4–4.3 eV range of organic semiconductors [31]. The substitution of aNDT makes E_g to narrowed, that determines kinetic stability and conductivity. aNDT and its functionalized molecules have an energy gap between 3.42 and 4.27 eV, with $–NO_2$ substituted molecule, aNDT3 having the smallest E_g value at 3.42 eV, followed by that –CN functionalized molecule, aNDT4 having the second least value of 3.91 eV, both of which are projected to have greater conductivity. Additionally, the $–NO_2$ and CN-functionalized molecules' LUMO energy levels also have the lowest values, which enhances the usefulness of aNDT as a conducting material. With the exception of the electron donating functionalized groups, C_2H_2 and OCH_3, all the HOMO and LUMO values inclined for aNDT1 and aNDT2 respectively. As seen in Fig. 3, the substitution of EDG on the aNDT molecule considerably raises the HOMO and LUMO energies. On the other hand, the substitution of EWGs considerably lowers the HOMO and LUMO energies.

The reactive sites of the molecule can be predicted using the electrostatic potential (ESP). Potential values outside of the minima and maxima defined in the color scale data range will be clamped to solid red and solid blue. aNDT, and their functionalized molecules' reactive sites are also depicted in Fig. 4. The addition of the functionalization generally led to an increase in reactivity in the site.

The significant effects of EDG and EWG on the aNDT and its derivative molecules were anticipated to have an impact on the absorption spectra of aNDT-unsub to aNDT4 molecules. Fig. 5 depicts the absorption spectra of the aNDT-based molecules that was estimated using the TD-DFT approach at the B3LYP/6–311+g(d,p) level of theory. To better understand the characteristics and energies of singlet-singlet electronic transitions, the first 10 low-lying electronic transition energies have been computed. Table 1 provides a summary of the calculated absorption wavelength, energy, oscillator strength, and associated electronic transitions. Throughout the discussion, the absorption transitions with oscillator strengths greater than 0.01 are taken into account. The excitation of an electron from HOMO to LUMO causes the lowest energy transition for all the molecules under study. The absorption spectrum ranges from 245 nm to 408 nm, which agrees well with the previously reported values for different compounds having potential applications in optoelectronics [9,14,20–22]. The aNDT molecule's highest absorption peak is visible at 245 and 322 nm, respectively, and these wavelengths correlate to the electronic transitions from HOMO-2 to LUMO+1, HOMO-1 to LUMO+2 and HOMO to LUMO. According to Fig. 5, the substitution of functional groups had a substantial impact on the absorption spectrum as evidenced by the change in the absorption maximum (λ_{max}) of aNDT1 to aNDT4 molecules. The maximum absorption wavelength of the functionalized molecules significantly redshifts from the unsubstituted aNDT molecule. For the aNDT3 molecule, a maximum redshift of 163 nm with respect to the aNDT-unsub molecule has been recorded. Followed by this, the second largest red shift of 105 nm was observed for aNDT4 molecule. The substitution of functional groups on the aNDT molecule resulted in an increase in the intensity of the λ_{max} peak.

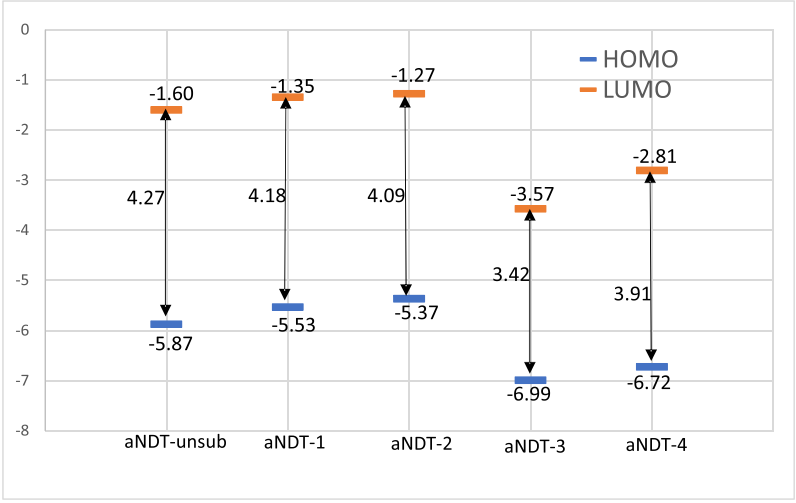

Fig. 3. Energy level diagram of the studied aNDT molecules obtained from B3LYP/6−311+G(d,p). The energy levels from HOMO (blue bars) to LUMO (Orange bars) are plotted. The EHOMO −ELUMO, energy gap (Eg) values are in eV. (For interpretation of the references to colour in this figure legend, the reader is referred to the Web version of this article.)

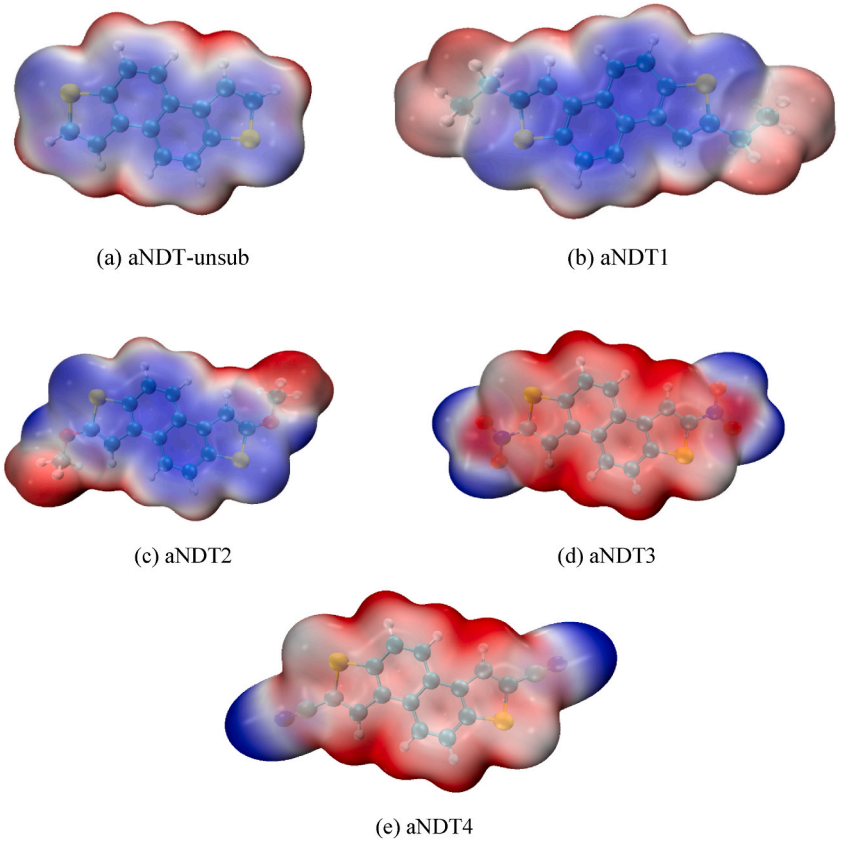

Fig. 4. ESP of aNDT (a) and its functionalized molecules (b–e).

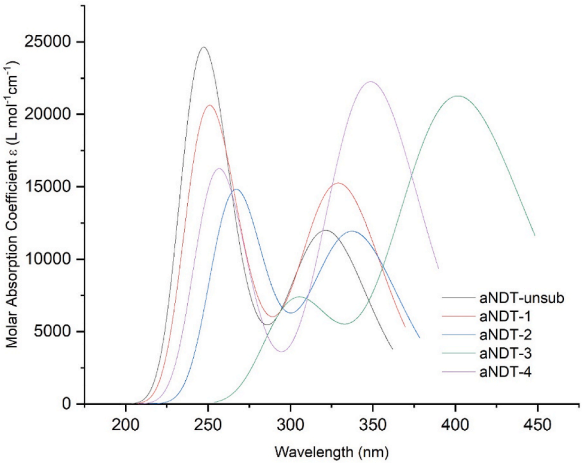

Fig. 5. Absorption spectrum of the studied aNDTs molecules calculated at the B3LYP/6−311+G(d,p) level of theory.

3.2. Ionization parameters

The calculated adiabatic/vertical ionization potentials (IP_A, IP_V), and the corresponding electron affinities (EA_A, EA_V), of the examined compounds based on B3LYP/6−311+G (d, p) levels are listed in Table 2. The findings demonstrate that the IPs and EAs sensitively depend on the basis set's diffuse function. The amount of structural relaxation following charge injection is indicated by the energy difference between the vertical and adiabatic values. The exothermicity for molecule reduction is indicated by the negative values of EAs. It is possible to effectively inject holes from the source electrode using a molecule with a small IP. A molecule with a good

Table 1
Calculated Absorption Energies (in eV), Wavelengths (in nm), Oscillator Strengths (in au), and the corresponding orbital transitions of studied aNDTs molecules calculated at the B3LYP/6−31+G(d,p) Level of Theory.

Molecules	Excitation Energy[a]		Oscillator strength	Orbital transitions
	Absorption energy (eV)	Absorption wavelength (nm)		
aNDT-unsub	3.85	322.03	0.28	HOMO→LUMO (88%)
	3.93	315.44	0.02	H-1→LUMO (72%), HOMO→L+2 (20%)
	4.76	260.31	0.14	H-1→LUMO (18%), HOMO→L+2 (68%)
	5.06	245.23	0.52	H-2→L+1 (13%), H-1→L+2 (74%)
aNDT1	3.76	329.66	0.36	HOMO→LUMO (94%)
	3.92	316.43	0.01	H-1→LUMO (70%), HOMO→L+2 (29%)
	4.67	265.55	0.15	H-1→LUMO (24%), HOMO→L+2 (62%)
	5.00	247.84	0.42	H-2→L+1 (22%), H-1→L+2 (64%)
aNDT2	3.66	338.50	0.28	HOMO→LUMO (95%)
	3.92	316.53	0.01	H-1→LUMO (54%), HOMO→L+1 (45%)
	4.64	267.07	0.35	H-1→LUMO (40%), HOMO→L+1 (48%)
	4.74	261.32	0.01	HOMO→L+5 (87%)
aNDT3	3.04	408.41	0.37	HOMO→LUMO (90%)
	3.20	387.55	0.18	H-1→LUMO (88%)
	4.07	304.66	0.18	H-2→L+1 (96%)
aNDT4	3.54	349.90	0.51	HOMO→LUMO (95%)
	3.70	334.69	0.05	H-1→LUMO (86%), HOMO→L+2 (12%)
	4.69	264.56	0.10	H-2→L+1 (18%), HOMO→L+2 (56%)
	4.79	258.86	0.11	H-2→L+1 (64%), HOMO→L+2 (17%)
	4.91	252.66	0.22	HOMO→L+3 (70%)

[a] Excitation energies were calculated in gas phase.

Table 2
The calculated vertical ionization potential (VIP), adiabatic ionization potential (AIP), vertical electron affinities (VEA), adiabatic electron affinities (AEA), electron extraction potential (EEP), hole extraction potential (HEP), hole reorganisation energy (λ_+), and electron reorganisation energy (λ_-) of the studied aNDT based molecules in eV.

Molecules	VIP	AIP	VEA	AEA	HEP	EEP	λ_-	λ_+
aNDT-unsub	7.37	7.25	0.14	0.28	7.12	0.42	0.28	0.25
aNDT1	6.93	6.80	−0.03	0.36	6.67	0.34	0.37	0.26
aNDT2	6.77	6.61	−0.13	0.02	6.44	0.17	0.30	0.33
aNDT3	8.40	8.27	2.24	2.41	8.14	2.58	0.34	0.25
aNDT4	8.10	8.01	1.46	1.60	7.90	1.73	0.27	0.20

ability to inject electrons will have a comparatively high electron affinity (EA). The vertical IPs of unsubstituted aNDT molecule having IP_v; 7.37 eV and IP_a; 7.25 eV are varied when different electron-donating and electron-withdrawing groups are added to the cyclopentane rings.

The IPs of molecules; aNDT1 and aNDT2 with electron donating functionalized groups [-C_2H_5 and –OCH_3] were declined from that of aNDT-unsub molecule. The corresponding adiabatic/vertical ionization potentials were 6.80/6.93 eV and 6.61/6.77 eV respectively. Thus it favours the hole injection from the metallic electrodes. aNDT3 with the nitrite (-NO_2) substituents has the highest IPs [8.27/8.40 eV] among the examined compounds. The fact that the vertical IPs of all molecules are greater than those of pentacene [32] (5.94 eV) and the stable p-type material sexithiophene [33] (5.80 eV) reveals that all of these molecules are more stable and have antioxidative properties in their natural environments. When compared to electron donating functionalized compounds with electron-withdrawing substituents, the EAs of molecules aNDT3 [2.24/2.41 eV] and aNDT4 [1.46/1.60 eV], showing that it is in favour of electron injection from the metallic electrodes. As seen in Fig. 3, aNDT3 and aNDT4 exhibits lower lying LUMO level than the other aNDT-based compounds, which increases its capacity to receive electrons. The HEP of the aNDT2 molecule (6.44 eV) has been found to be lower than that of other analyzed molecules, demonstrating that the injection of an electron into the cationic geometry of the aNDT2 molecule is easier than that of the other studied molecules. Also, the EEP of the aNDT1 and aNDT2 are smaller. According to Koopman's theorem [34], the trend in the difference between IP and EA is consistent with the computed FMO energy gap (E_g).

3.3. Reorganisation energies

The treatment of reorganisation energies as a significant factor that affects the charge mobility of organic semiconductors. In both adiabatic and vertical form using the B3LYP/6−311+G(d,p) theory of level, the reorganisation energies of the investigated compounds were determined. The results are tabulated in Table 2. Here, we took into account that the external environment makes a negligible contribution to the reorganisation energy. The values in Table 2 provided show that the investigated compounds' hole and electron reorganisation energies differ dramatically when various substituents are added to the core of the cyclopentane rings of aNDT molecule. The examined molecule aNDT have internal electron and hole reorganisation energies, of 0.28 eV and 0.25 eV, respectively.

According to a report [35], higher charge transport is not recommended by larger reorganisation energy values. Except, aNDT2, the reorganisation energies for the hole, λ_+ of all aNDT molecules are lower than those for the electron suggests that these molecules may aid in the transport of the hole. The maximum electron reorganisation energy, λ_- was calculated for aNDT1 molecule which favours the hole transportation process.

The root mean square deviation (RMSD) between the internal coordinates of neutral and cationic/anionic geometry of the researched molecules was used to estimate the studied reorganisation energies corresponding to excess positive or negative charges on the molecules.

The higher λ_- value for aNDT1 was supported from RMSD between its neutral and anionic geometries which is 0.93, whereas it is 0.02 for other studied molecules. With respect to neutral geometry, it has been found that the RMSD value for the methoxy-(OCH_3) substituted molecule, aNDT2 is 0.03 for both positive and negative charges. As a result, the aNDT2 molecule works well for ambipolar charge transfer semiconductors.

3.4. Crystal structures of aNDT's

The design and synthesis of organic semiconductors, as well as recognising the structure-property relationship and the limits of charge transport, are all enhanced from an understanding of the molecular packing features [36]. An organic crystal is a regular arrangement of similar molecules held together by van der Waals forces, hydrogen bonds, and other intermolecular forces. In addition to the composition of the molecule itself, the molecular packing motifs should have strong intermolecular interactions in order to ensure effective charge transfer and, consequently, the high performance of organic semiconductor crystals. As there is no crystal structure report for the subjected aNDT derivatives, using their optimum gas-phase conformations, the Polymorph Predictor module of the Materials Studio package (17.1.0.48) [37] has predicted the crystal structures of the aNDT-systems. The Polymorph Predictor quality was set to the default fine setting for this calculation, which anneals the sample using the Monte Carlo simulation algorithm [38] between 300.0 K and 100000.0 K with a heating factor of 0.025. The maximum number of steps in this algorithm is 7000, and 12 consecutive steps are tolerated before cooling. Here, we've combined Gasteiger charges with the Dreiding forcefield. We limit our estimate to the ten most prevalent space groups of organic compounds as documented in the Cambridge Structural Database ($P2_1/c$, P1, $P2_12_12_1$, C2/c, $P2_1$, Pbca, $Pna2_1$, Pbcn, and C2). The crystal structures have been sorted according to their total energies, and the lowest structure was used for further calculations. The crystal parameters of aNDT and functionalized aNDT's were summarized in Table 3. The comparison of lattice parameters of predicted aNDT-unsub crystal structure with that of the similar structure reported experimentally [9], was carried out in-order to validate the prediction methodology. It was found that the average deviation of about 7% was calculated, and the comparison table was appended as supplementary information as Table S2.

The molecular packing motifs of aNDT and their derivatives were shown in Fig. 6. The typical packing motifs in the crystal structure of aNDT-unsub are lamellar packing motif, two dimensional (2D) π– π stacking, aNDT1 are lamellar packing motif with two dimensional (2D) π–π stacking, aNDT2 are herringbone packing motif without π–π overlap (face-to-face) between adjacent molecules, aNDT3 are herringbone packing motif with π–π overlap between adjacent molecules and aNDT4 are lamellar packing motif, two dimensional (2D) π–π stacking. The π–π stacking has been considered to be the most effective packing method for transporting charge carriers [39]. Hirshfeld analysis was carried out to estimate the intermolecular interactions which heavily influence the molecular packing properties.

3.5. Hirshfeld surface analysis

By using various colours and intensities in graphical representation, the Hirshfeld surface analysis helps to quantify and visualise intermolecular interactions. Numerous intermolecular interactions have been examined using Hirshfeld surface analysis in the crystal structure of organic molecules and complexes [40,41]. Fig. 7 shows the d_{norm} (normalised contact distance) maps of aNDT and their functionalized molecules. Red surfaces show connections that are closer together than the van der Waals radii, while blue surfaces represent interactions that are farther apart (distance contact). van der Waals radii added together represent the distance indicated by the white surfaces. The –NO_2 groups in the aNDT3 molecule appear to be the source of the red areas. In intermolecular interactions, the red areas of the molecules may function as donors. It is anticipated that more donor sites will cling to their functionalized molecules with electronegative groups as a result. Fig. 7 also displays the shape-index of aNDTs on the Hirshfeld surface. The neighbouring red and blue triangles indicate the π-π stacking interaction between the structures. The red and blue sections represent the donor and acceptor groups of the molecule. Fig. 8 show, respectively, the 2D fingerprint plots and fragment patches of aNDT's. The d_e and d_i on the plots stand for the external and interior distances from the surface to the closest atom centre, respectively. Plot spots without a

Table 3
The unit cell parameters of predicted crystal structures of aNDT based molecule.

Structure	Space group	a(Å)	b(Å)	c(Å)	α(°)	β(°)	γ(°)	Volume (Å^3)
aNDT-unsub	$P2_1/c$	18.316	8.910	7.000	90.0	83.8	90.0	1134.0
aNDT1	$P2_1/c$	4.026	24.023	22.795	90.0	43.0	90.0	1503.6
aNDT2	$P2_1/c$	8.232	19.832	8.582	90.0	96.4	90.0	1392.3
aNDT3	$P2_1$	16.996	6.068	6.826	90.0	66.5	90.0	645.6
aNDT4	$P2_1$	4.044	10.557	18.205	90.0	55.2	90.0	637.9

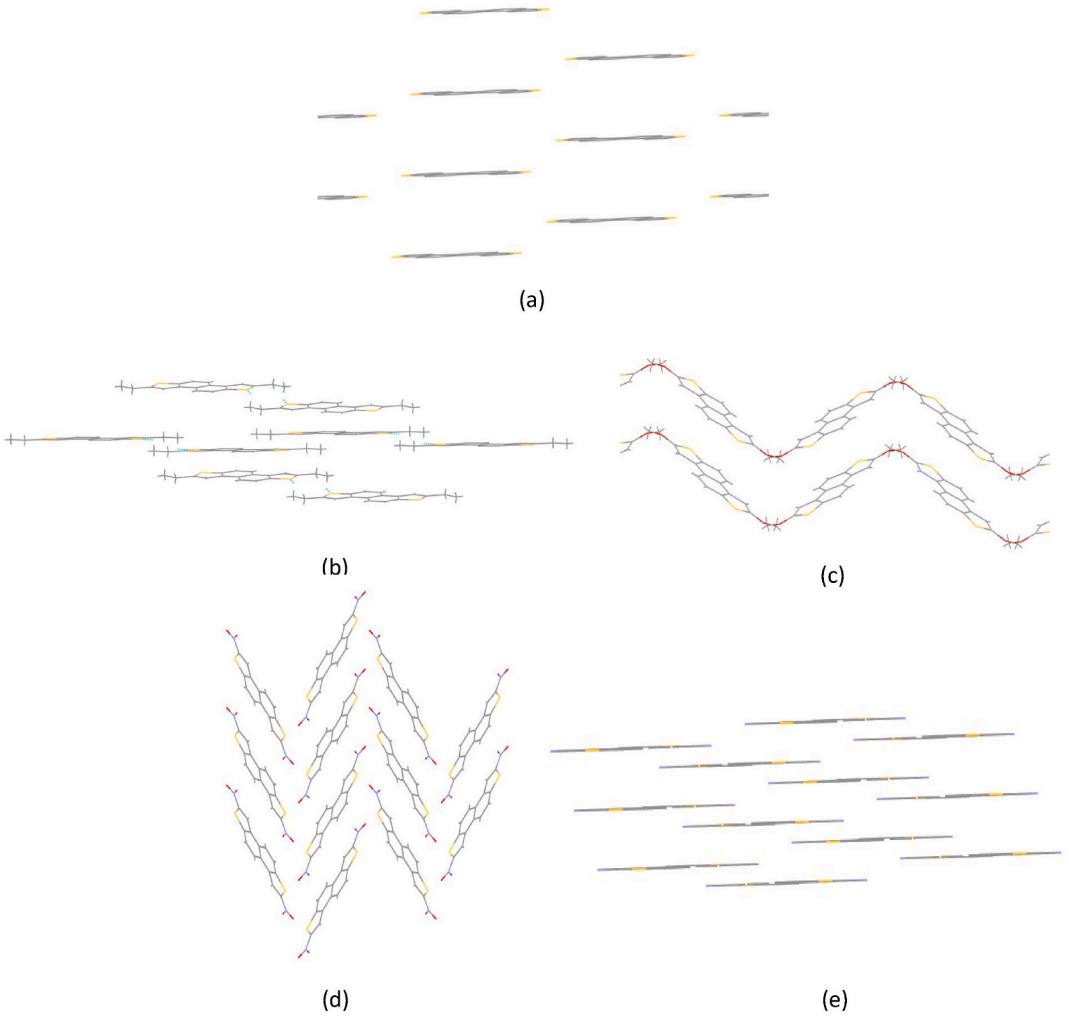

Fig. 6. Molecular packing motifs of aNDT systems (a–e).

contribution are grey, while those with a little contribution range from blue to green to red for those with the biggest contributions. Except, aNDT4, H···H interaction makes significant contribution in overall surface of all aNDTs. Next to H···H interactions, S···H/H···S interactions were the second largest contributions in aNDT-unsub, aNDT1 and aNDT2 molecules. As expected, in electron withdrawing functionalized substituted molecules, aNDT3 and aNDT4, the O···H/H···O [19.7%] and N···H/H···N [27.6%] were highly dominated in the Hirshfeld surface. Other minor contributions were displayed in Fig. S1.

4. Conclusion

Electronic and, optical characteristics, in angular naphthodithiophene (aNDT) based molecules are investigated for the different functional group substitution. Electron-donating groups (EDGs) and electron-withdrawing groups (EWGs) were substituted onto the 2 and 7 positions of aNDT molecule. When a functional group was substituted, it altered the energy levels of the molecule, which led to a significant variation in the absorption spectra compared to the unsubstituted aNDT molecule. Absorption spectra were determined, and they show that the aNDT molecules have potential applications in optoelectronics. The p-type characteristics of $–C_2H_5$ [aNDT1] and –CN [aNDT4] substituted aNDT molecules was well reflected from its highest λ_{-}; 0.37 and lowest λ_{+}; 0.20 values. The RMSD value for the methoxy-(OCH_3) substituted molecule, aNDT2, is found to be 0.03 for both positive and negative charges, indicating that the aNDT2 molecules are useful for ambipolar charge transfer semiconductors. Hirshfeld surface analysis was also used to learn about the intermolecular interactions in aNDT molecules. When analysing the 3D energy structure of aNDTs crystals, it was discovered that the O···H/H···O, S···H/H···S and N···H/H···N interactions were the dominating one. Thus, new organic semiconductors for optoelectronic applications are highlighted by this work.

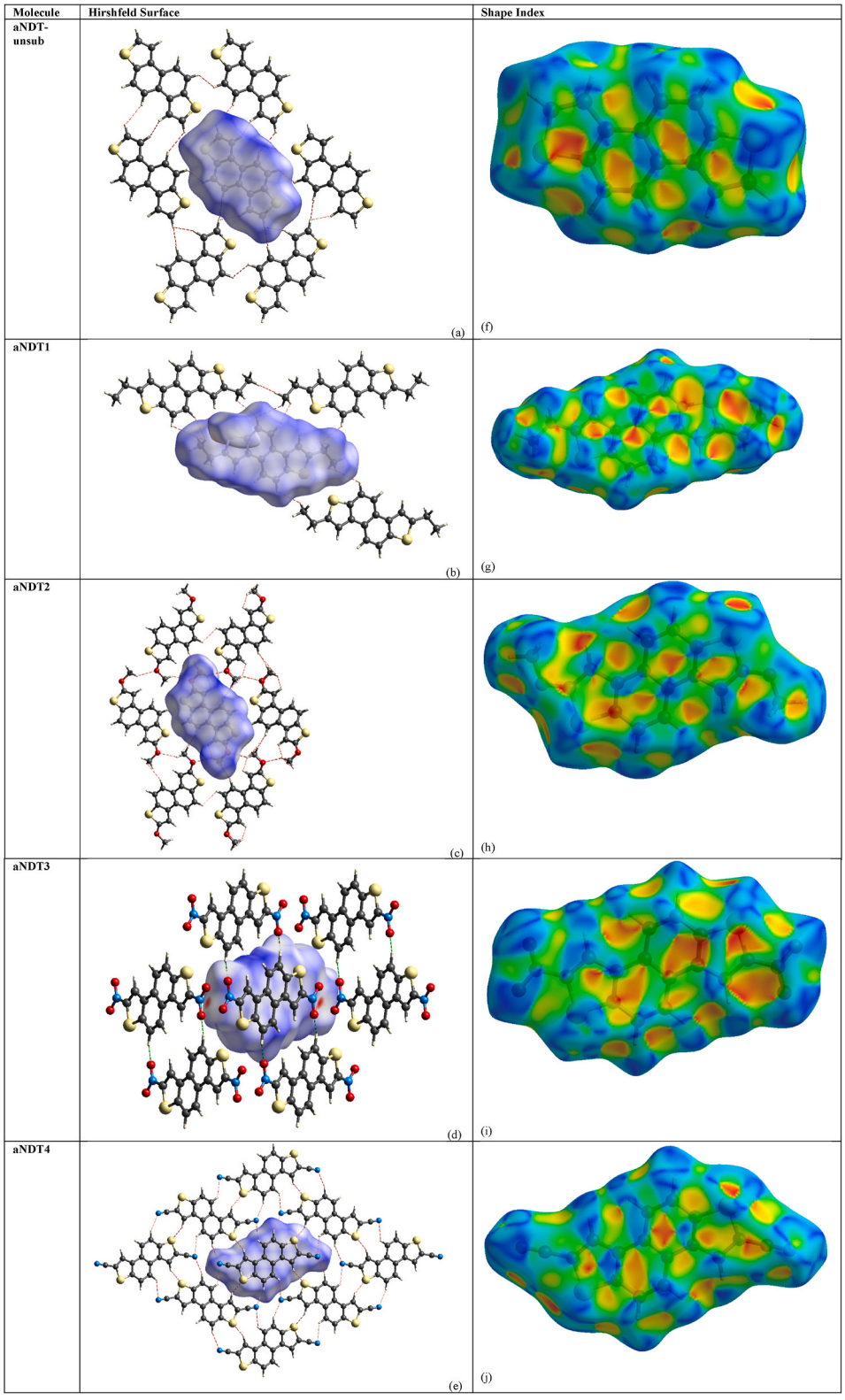

Fig. 7. Hirshfeld surface (a–e) of and Shape-index (f–j) plotted over d_{norm} of aNDTs systems.

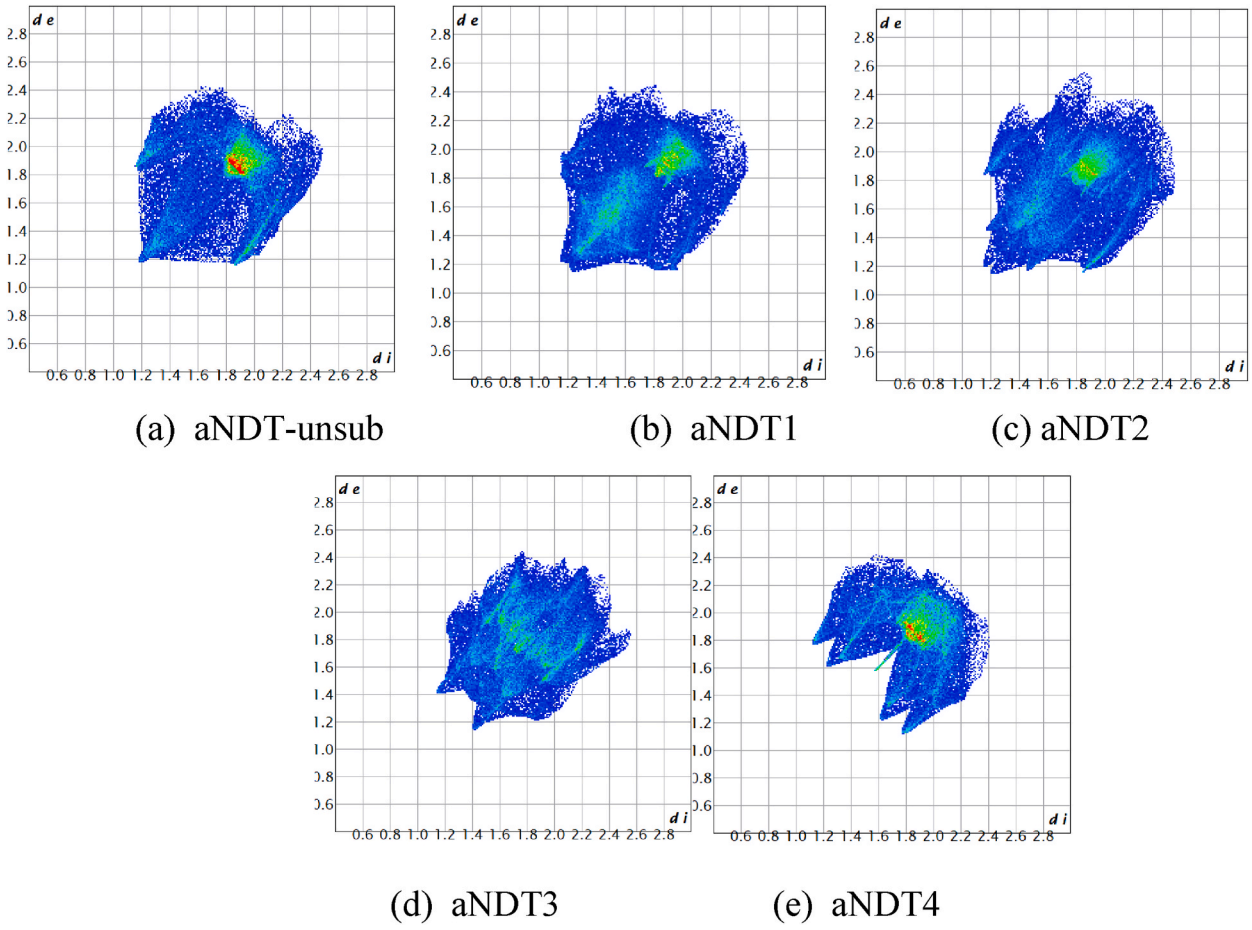

Fig. 8. Two-dimensional fingerprint plots of aNDTs (a–e) for intermolecular interactions.

Author contribution statement

B. Jothi: Performed the experiments; Analyzed and interpreted the data; Wrote the paper.
A. David Stephen: Analyzed and interpreted the data; Contributed reagents, materials, analysis tools or data; Wrote the paper.
K. Selvaraju: Conceived and designed the experiments; Analyzed and interpreted the data; Wrote the paper.
Abdullah G Al-Sehemi: Performed the experiments; Contributed reagents, materials, analysis tools or data; Wrote the paper.

Data availability statement

Data will be made available on request.

Declaration of competing interest

The authors declare that they have no known competing financial interests or personal relationships that could have appeared to influence the work reported in this paper

Acknowledgement

The Deanship of scientific research at King Khalid university is greatly appreciated for funding (R. G. P-2/67/44).

Appendix A. Supplementary data

Supplementary data to this article can be found online at https://doi.org/10.1016/j.heliyon.2023.e16740.

References

[1] F. Yang, Y. Huang, Y. Li, Y. Li, Large-area flexible organic solar cells, npj Flex. Electron. 5 (2021) 30.
[2] K. Liu, B. Ouyang, X. Guo, Y. Guo, Y. Liu, Advances in flexible organic field-effect transistors and their applications for flexible electronics, npj Flex. Electron. 6 (2022).
[3] M. Riede, D. Spoltore, K. Leo, Organic solar cells—the path to commercial success, Adv. Energy Mater. 11 (2020), 2002653.
[4] F. Liu, L. Zhou, W. Liu, Z. Zhou, Q. Yue, W. Zheng, R. Sun, W. Liu, S. Xu, H. Fan, L. Feng, Y. Yi, W. Zhang, X. Zhu, Organic solar cells with 18% efficiency enabled by an alloy acceptor: a two-in-one strategy, Adv. Mater. 33 (2021), 2100830.
[5] C. Li, J. Zhou, J. Song, J. Xu, H. Zhang, X. Zhang, J. Guo, L. Zhu, D. Wei, G. Han, J. Min, Y. Zhang, Z. Xie, Y. Yi, H. Yan, F. Gao, F. Liu, Y. Sun, Non-fullerene acceptors with branched side chains and improved molecular packing to exceed 18% efficiency in organic solar cells, Nat. Energy 6 (2021) 605–613.
[6] K. Jin, Z. Xiao, L. Ding, 18.69% PCE from organic solar cells, J. Semiconduct. 42 (2021), 060502.
[7] Y. Firdaus, V.M. Le Corre, J.I. Khan, Z. Kan, F. Laquai, P.M. Beaujuge, T.D. Anthopoulos, Key parameters requirements for non-fullerene-based organic solar cells with power conversion efficiency >20, Adv. Sci. (Weinh) 6 (2019) 1802028.
[8] N. Hossain, S. Das, T.L. Alford, An approach to equivalent circuit modelling of inverted organic solar cells, Circ. Syst. 7 (2016) 1297–1306.
[9] S. Shinamura, I. Osaka, E. Miyazaki, A. Nakao, M. Yamagishi, J. Takeya, K. Takimiya, Linear- and angular-shaped naphthodithiophenes: selective synthesis, properties, and application to organic field-effect transistors, J. Am. Chem. Soc. 133 (2011) 5024–5035.
[10] I. Osaka, T. Abe, S. Shinamura, K. Takimiya, Impact of isomeric structures on transistor performances in naphthodithiophene semiconducting polymers, J. Am. Chem. Soc. 133 (2011) 6852–6860.
[11] S. Li, J. Yuan, P. Deng, W. Ma, Q. Zhang, Synthesis and photovoltaic properties of new conjugated polymers based on two angular-shaped naphthodifuran isomers and isoindigo, Sol. Energy Mater. Sol. Cell. 118 (2013) 22–29.
[12] L. Wang, J. Dai, Y. Song, Theoretical investigations of the substituent effect on the electronic and charge transport properties of butterfly molecules, New J. Chem. 43 (2019) 12440–12452.
[13] M. Vadivel, S. Singh, D.P. Singh, V.A. Raghunathan, S. Kumar, Ambipolar charge transport properties of naphthophenanthridine discotic liquid crystals, J. Phys. Chem. B 125 (2021) 10364–10372.
[14] M. Pavithrakumar, S. Krishnan, K. Senthilkumar, Charge transport and optical absorption properties of dibenzocoronene tetracarboxdiimide based liquid crystalline molecules: a theoretical study, J. Phys. Chem. A 125 (2021) 3852–3862.
[15] S. Shinamura, R. Sugimoto, N. Yanai, N. Takemura, T. Kashiki, I. Osaka, E. Miyazaki, K. Takimiya, Orthogonally functionalized naphthodithiophenes: selective protection and borylation, Org. Lett. 14 (2012) 4718–4721.
[16] M. Nakano, S. Shinamura, R. Sugimoto, I. Osaka, E. Miyazaki, K. Takimiya, Borylation on benzo[1,2-b:4,5-b']- and naphtho[1,2-b:5,6-b′]dichalcogenophenes: different chalcogene atom effects on borylation reaction depending on fused ring structure, Org. Lett. 14 (2012) 5448–5451.
[17] I. Osaka, T. Abe, M. Shimawaki, T. Koganezawa, K. Takimiya, Naphthodithiophene-based donor–acceptor polymers: versatile semiconductors for OFETs and OPVs, ACS Macro Lett. 1 (2012) 437–440.
[18] S. Shi, X. Xie, P. Jiang, S. Chen, L. Wang, M. Wang, H. Wang, X. Li, G. Yu, Y. Li, Naphtho[1,2-b:5,6-b′]dithiophene-Based donor–acceptor copolymer semiconductors for high-mobility field-effect transistors and efficient polymer solar cells, Macromolecules 46 (2013) 3358–3366.
[19] S. Shi, P. Jiang, S. Yu, L. Wang, X. Wang, M. Wang, H. Wang, Y. Li, X. Li, Efficient polymer solar cells based on a broad bandgap D–A copolymer of "zigzag" naphthodithiophene and thieno[3,4-c]pyrrole-4,6-dione, J. Mater. Chem. A 1 (2013) 1540–1543.
[20] S. Debata, S.R. Sahoo, R. Khatua, S. Sahu, Rational design and crystal structure prediction of ring-fused double-PDI compounds as n-channel organic semiconductors: a DFT study, Phys. Chem. Chem. Phys. 23 (2021) 12329–12339.
[21] J. Vollbrecht, C. Wiebeler, H. Bock, S. Schumacher, H.-S. Kitzerow, Curved polar dibenzocoronene esters and imides versus their planar centrosymmetric homologs: photophysical and optoelectronic analysis, J. Phys. Chem. C 123 (2019) 4483–4492.
[22] S. Shinamura, E. Miyazaki, K. Takimiya, Synthesis, properties, crystal structures, and semiconductor characteristics of naphtho[1,2-b:5,6-b′]dithiophene and -diselenophene derivatives, J. Org. Chem. 75 (2010) 1228–1234.
[23] C. Lee, W. Yang, R.G. Parr, Development of the Colle-Salvetti correlation-energy formula into a functional of the electron density, Phys. Rev. B 37 (1988) 785–789.
[24] A.D. Becke, Density-functional thermochemistry. I. The effect of the exchange-only gradient correction, J. Chem. Phys. 96 (1992) 2155–2160.
[25] A.D. Becke, Density-functional exchange-energy approximation with correct asymptotic behavior, Phys. Rev. A 38 (1988) 3098–3100.
[26] H.L. Tavernier, M.D. Fayer, Distance dependence of electron transfer in DNA: the role of the reorganization energy and free energy, J. Phys. Chem. B 104 (2000) 11541–11550.
[27] R. Nithya, M. Sowmiya, P. Kolandaivel, K. Senthilkumar, Structural, optical, and charge transport properties of cyclopentadithiophene derivatives: a theoretical study, Struct. Chem. 25 (2014) 715–731.
[28] M. Frisch, G.W. Trucks, H.B. Schlegel, G.E. Scuseria, M.A. Robb, J.R. Cheeseman, G. Scalmani, V. Barone, B. Mennucci, G. Petersson, Gaussian 09, Revision d. 01, Gaussian, Inc., Wallingford CT, 2009, p. 201.
[29] M.A. Spackman, D. Jayatilaka, Hirshfeld surface analysis, CrystEngComm 11 (2009) 19–32.
[30] P.R. Spackman, M.J. Turner, J.J. McKinnon, S.K. Wolff, D.J. Grimwood, D. Jayatilaka, M.A. Spackman, CrystalExplorer: a program for Hirshfeld surface analysis, visualization and quantitative analysis of molecular crystals, J. Appl. Crystallogr. 54 (2021) 1006–1011.
[31] Z. Chen, Z. He, Y. Xu, W. Yu, Density functional theory calculations of charge transport properties of 'plate-like' coronene topological structures, J. Chem. Sci. 129 (2017) 1341–1347.
[32] L. Wang, T. Li, Y. Shen, Y. Song, A theoretical study of the electronic structure and charge transport properties of thieno[2,3-b]benzothiophene based derivatives, Phys. Chem. Chem. Phys. 18 (2016) 8401–8411.
[33] J.-D. Huang, S.-H. Wen, W.-Q. Deng, K.-L. Han, Simulation of hole mobility in α-oligofuran crystals, J. Phys. Chem. B 115 (2011) 2140–2147.
[34] T. Koopmans, Über die Zuordnung von Wellenfunktionen und Eigenwerten zu den Einzelnen Elektronen Eines Atoms, Physica 1 (1934) 104–113.
[35] C.I.L. Alongamo, S.N. Tasheh, N.K. Nkungli, F.K. Bine, J.N. Ghogomu, Structural, electronic, and charge transport properties of new materials based on 2-(5-mercapto-1,3,4-oxadiazol-2-yl) phenol for organic solar cells and light emitting diodes by DFT and TD-DFT, J. Chem. 2022 (2022) 1–15.
[36] Y.-R. Shi, H.-L. Wei, X.-B. Jia, Y.-F. Liu, Effects of crystal structures and intermolecular interactions on charge transport properties of organic semiconductors, J. Mater. Sci. 53 (2018) 15569–15587.
[37] M. Accelrys, Materials Studio is a Software Environment for Molecular, Dassault Systèmes BIOVIA, 2009.
[38] S.C. Howell, X. Qiu, J.E. Curtis, Monte Carlo simulation algorithm for B-DNA, J. Comput. Chem. 37 (2016) 2553–2563.
[39] C. Wang, H. Dong, L. Jiang, W. Hu, Organic semiconductor crystals, Chem. Soc. Rev. 47 (2018) 422–500.
[40] P.V. Thong, N.T.T. Chi, M. Azam, C.H. Hanh, L.T.H. Hai, L.T. Duyen, M. Alam, S.I. Al-Resayes, N.V. Hai, NMR investigations on a series of diplatinum(II) complexes possessing phenylpropanoids in CDCl3 and CD3CN: crystal structure of a mononuclear platinum complex, Polyhedron 212 (2022), 115612.
[41] S.I. Al-Resayes, M. Azam, A. Trzesowska-Kruszynska, R. Kruszynski, S.M. Soliman, R.K. Mohapatra, Z. Khan, Structural and theoretical investigations, Hirshfeld surface analyses, and cytotoxicity of a naphthalene-based chiral compound, ACS Omega 5 (2020) 27227–27234.